The plastome-encoded PsaJ subunit is required for efficient Photosystem I excitation, but not for plastocyanin oxidation in tobacco

Mark A Schöttler, Claudia Flügel, Wolfram Thiele, Sandra Stegemann, Ralph Bock

Biochemical Journal Immediate Publication. Published on 9 Jan 2007 as manuscript BJ20061573

The plastome-encoded PsaJ subunit is required for efficient photosystem I excitation, but not for plastocyanin oxidation in tobacco

Authors´ names: Mark A. Schöttler[1], Claudia Flügel, Wolfram Thiele, Sandra Stegemann, Ralph Bock

Establishment address: Max-Planck-Institut für Molekulare Pflanzenphysiologie, Am Mühlenberg 1, D-14476 Potsdam-Golm, Germany

Page heading title: PsaJ functions in photosystem I excitation

[1]Corresponding author: Mark Aurel Schöttler
e-mail address: schoettler@mpimp-golm.mpg.de
Fax: +49-331-567-8701

Abbreviations used: chl. – chlorophyll; CTAB – cetyltrimethylammoniumbromide; cyt – cytochrome; cyt-bf – cytochrome-b_6f complex; DDM – β-dodecylmaltoside; EP – electron pairs; P_{700} - chlorophyll-a dimer of the PSI reaction center; PC – plastocyanin; PQ – plastoquinone; PS – photosystem; TMPD – tetramethyl-1,4-phenylendiamine; WT – wild type

Key words: photosynthesis, photosystem I, PsaJ, plastocyanin, Lhca

Biochemical Journal Immediate Publication. Published on 9 Jan 2007 as manuscript BJ20061573

The functions of several small subunits of the large photosynthetic multiprotein complex photosystem I (PSI) are not yet understood. To elucidate the function of the small plastome-encoded PsaJ subunit, we have produced knock-out mutants by chloroplast transformation in tobacco (*Nicotiana tabacum*). PsaJ binds 2 chlorophyll-a molecules and is localized at the periphery of PSI, close to both the Lhca2 and Lhca3 docking sites and the plastocyanin binding site. Tobacco *psaJ* knock-out lines do not display a visible phenotype. Despite a 25% reduction in the content of redox-active PSI, neither growth rate nor assimilation capacity are altered in the mutants. *In vivo*, redox equilibration of plastocyanin and PSI is as efficient as in the wild type, indicating that PsaJ is not required for fast plastocyanin oxidation. However, PsaJ is involved in PSI excitation: Altered 77 K chlorophyll-a fluorescence emission spectra and reduced accumulation of Lhca3 indicate that antenna binding and exciton transfer to the PSI reaction center are impaired in Δ*psaJ* mutants. Under limiting light intensities, growth of Δ*psaJ* plants is retarded and the electron transport chain is far more reduced than in the wild type, indicating that PSI excitation might limit electron flux at sub-saturating light intensities. In addition to defining *in vivo* functions of PsaJ, our data may also have implications for the interpretation of the crystal structure of PSI.

Introduction: Photosystem I (PSI) is a multisubunit protein complex in the photosynthetic membranes of higher plants, algae and cyanobacteria. It consists of 15 core subunits and 5 different antenna proteins in higher plants [1,2]. PSI catalyzes the final step of linear electron transport, the light-driven oxidation of plastocyanin (PC) and the reduction of ferredoxin. Despite the existence of a crystal structure of higher plant PSI [3], the exact functions of several subunits are still unknown. Best understood is the role of the three plastome-encoded subunits PsaA, PsaB and PsaC, which are essential for PSI assembly and function, because they bind all redox-active cofactors: PsaA and PsaB form the PSI reaction center heterodimer and bind the majority of the cofactors and antenna chlorophylls (chl.), whereas PsaC binds the cofactors F_A and F_B on the PSI acceptor side. In the absence of any of these subunits, functional PSI cannot accumulate in photosynthetic eukaryotes [4,5].

In higher plants, the function of the nuclear-encoded subunits has been elucidated in recent years using RNAi, antisense techniques and insertional mutagenesis in *Arabidopsis thaliana* (reviewed in [6,7]). This work has revealed non-essential functions of most nuclear-encoded PSI subunits, with the exception of PsaD, which is essential for PSI accumulation and is involved in the formation of the ferredoxin-binding site [8,9]. All other knock-out mutants displayed much weaker phenotypes, often including a reduced PSI content due to destabilization of the complex and sometimes showing altered antenna binding and exciton transfer to the reaction center [10-12].

In contrast, the functions of the plastome-encoded small PSI subunits, PsaI and PsaJ, has not yet been resolved in higher plants. In the unicellular green alga *Chlamydomonas reinhardtii*, PsaJ is required for the stabilization of the PC-binding site [13]. In the absence of PsaJ, a large fraction of photooxidized P_{700} is not efficiently reduced by PC or cytochrome c_6, although the PsaF subunit, which forms the actual binding site for both mobile redox carriers, is still present. This has suggested a role of PsaJ in adjusting the conformation of the PC binding site. These physiological data are circumstantially supported by structural data [3] and cross-linking studies [14] revealing a localization of the J-subunit adjacent to PsaF. Furthermore, in a Synechocystis Δ*psaJ* mutant, PsaF and PC binding were also affected [15]. In addition, as PsaJ is known to bind 2 chl.-a molecules in higher plants [16] and is also localized close to the binding sites of the Lhca2 and Lhca3 antenna proteins, an involvement in exciton transfer to the PSI reaction center has been proposed [16]. However, this hypothesis has not yet been addressed experimentally in any photosynthetic eukaryote.

To investigate both the possible role of PsaJ in the interaction between PC and PSI and the proposed function in light harvesting, we have constructed a *psaJ* knockout mutant in tobacco (*Nicotiana tabacum* L.). The availability of a workable chloroplast transformation technology for tobacco plants facilitates the construction of knock-out mutants for plastome-encoded genes and open reading frames [17,18]. The wild-type (WT) copy of the gene of interest is replaced by homologous recombination with a knock-out allele generated by gene disruption with a selectable marker, most often the *aadA* gene conferring resistance to the aminoglycoside antibiotics spectinomycin and streptomycin [19,20]. Analyzing a *psaJ* knockout transformant, we demonstrate here that the PsaJ

protein is not required for efficient PC oxidation under physiological conditions, but that it is instead involved in exciton transfer to the PSI reaction center.

Experimental

Plant growth - WT tobacco (*Nicotiana tabacum* L. var. Petit Havana) and the Δ*psaJ* transformants were grown on soil in controlled environment chambers at approximately 600 µE m^{-2} s^{-1} light intensity at the uppermost leaves. The day length was set to 16 h, day temperature was 22° C, relative humidity 75%. Night temperature was 18°C, relative humidity was decreased to 70%. For low-light experiments, the growth conditions were as stated above, except that the light intensity was reduced to 20 µE m^{-2} s^{-1}.

Vector construction and chloroplast transformation - Plastid transformation vector pΔpsaJ was derived from a cloned tobacco ptDNA fragment. A 1871 bp SpeI restriction fragment was subcloned into the unique SpeI site of vector pBluescript SK+ which had been dephosphorylated after linearization by treatment with calf intestinal phosphatase. The *psaJ* reading frame was disrupted by partial digestion with BglII and recovery of the linearized fragment followed by blunting of the overhanging ends by a fill-in reaction with the Klenow fragment of DNA polymerase I from *E. coli* (New England BioLabs). Subsequently, a chimeric *aadA* gene [21] was inserted as a blunt-end Ecl136II/DraI fragment into the blunted BglII site within the *psaJ* coding region. A clone was selected that contained the plastid selectable marker gene *aadA* in the same transcriptional orientation as the *psaJ* gene. This clone was designated pΔpsaJ and used as chloroplast transformation vector.

Young leaves from sterile tobacco plants were bombarded with plasmid pΔpsaJ-coated 0.6 µm gold particles using a biolistic gun (PDS1000He; BioRad). Primary spectinomycin-resistant lines were selected on RMOP regeneration medium containing 500 mg/l spectinomycin [21]. Spontaneous spectinomycin-resistant plants were eliminated by double selection on medium containing spectinomycin and streptomycin (500 mg/l each; 21, 22). Several independent transplastomic lines were subjected to three additional rounds of regeneration on RMOP/spectinomycin to enrich the transplastome and isolate homoplasmic *psaJ* knock-out lines.

Isolation of nucleic acids, polymerase chain reactions (PCR) and DNA gel blot analyses - Total plant nucleic acids were isolated from leaf tissue samples by a cetyltrimethylammoniumbromide (CTAB)-based method. For gel blot experiments, DNA samples were digested with restriction enzymes, separated on 0.8 % agarose gels and blotted onto Hybond N nylon membranes (Amersham Biosciences, Little Chelfont, UK). For hybridization, α[^{32}P]dATP-labeled probes were generated by random priming (Multiprime DNA labeling kit, Amersham). A PCR product covering the entire *psaJ* coding region (generated with primers PpsaJf 5' GGTTTTTCAATGCGAGATCTA 3' and PpsaJr 5' CATGACAATAACTAGAATGAA 3') was used as probe for the restriction fragment length polymorphism (RFLP) analyses. Hybridizations were carried out at 65°C in Rapid Hybridization

Buffer (Amersham) following the manufacturer's protocol. DNA samples were amplified with *psaJ*-specific primers in an Eppendorf thermocycler using Taq DNA polymerase (Promega) and standard protocols (50 ng total genomic DNA in 50 µl reactions). The PCR program was 35 cycles of 45 s at 94°C, 90 s at 56°C and 90 s at 72°C with a 4 min extension of the first cycle at 94°C and a 6 min final extension at 72°C. PCR products were analyzed by electrophoretic separation in 1.5 % agarose gels.

Gas exchange measurements - Leaf assimilation capacity was determined in saturating light (800 µE m^{-2} s^{-1}, generated by a tungsten halogen lamp, Schott, Mainz, Germany) in a closed cuvette system with a Clark-type oxygen electrode (LD-2, Hansatech, Norfolk, GB). Leaf discs (10 cm^2 surface area) were measured in a CO_2-enriched atmosphere (10% CO_2), to completely suppress photorespiration. Assimilation was measured until steady state. The chl. content of the leaf discs was determined after extraction in 80% acetone [22]. Assimilation rates were corrected for dark respiration, assuming comparable respiration rates in the light as in darkness [23]. It was shown previously that the assimilation capacity determined under these conditions closely correlates with the maximum capacity of linear electron flux [24].

Thylakoid membrane isolation and treatments with chaotropic agents - Thylakoid membranes were isolated as described [24]. The chl. contents and a/b ratio were determined in 80% acetone [22]. For the *in vitro* stability measurements of PSI, thylakoid membranes equivalent to 200 µg chl. ml^{-1} were incubated in medium A (5 mM $MgCl_2$, 30 mM KCl, 40 mM HEPES, pH 7.6) as a control or in medium A containing either 1 M NaCl, 2 M KI or 2 M NaBr. After 10 min of incubation in the chaotropic salt solution, thylakoids were sedimented by centrifugation (10.000 x g for 1 min) and resuspended in medium A.

Fluorometry - The 77 K chl.-a fluorescence emission spectra were measured using a Jasco F6500 fluorometer with a red-sensitive photomultiplier. Samples equivalent to 10 µg chl. ml^{-1} were excited at 430 nm wavelength (10 nm bandwidth), and emission spectra were measured from 660 to 800 nm wavelength with 0.5 nm steps and a bandwidth of 1 nm. The spectra were corrected for the instrumental response of the photomultiplier.

Room temperature chl.-a fluorescence of leaves was measured using a Dual-PAM instrument (Walz, Effeltrich, Germany). The redox state of Q_A and of the PQ pool was calculated from (1-qL), a parameter more accurate than the commonly used (1-qP) [25]. To determine the capacity for state transitions, leaves were excited using a red light LED (λ = 660 nm, 80 µE m^{-2} s^{-1} light intensity) and either blue light for predominant PSII excitation and PQ pool reduction (λ = 440 nm, 25 µE m^{-2} s^{-1}) or far-red light (λ = 715 nm) for preferential excitation of PSI and PQ pool oxidation. Measurements were performed and analyzed according to [26].

Cyt-bf and PSII quantification - The cytochromes of the thylakoid membrane were determined in isolated thylakoids equivalent to 50 µg chl. ml^{-1} after destacking in a low-salt medium, to improve the optical properties of the sample [27]. The cytochromes were oxidized by addition of 1 mM ferricyanide and subsequently reduced by addition of 10 mM ascorbate and dithionite, resulting in

reduction of cyt-f and the high potential form of cyt b_{559} (HP, ascorbate – ferricyanide difference absorption spectrum) and reduction of cyt-b_6 and the low-potential form of cyt-b_{559} (LP, dithionite – ascorbate), respectively. At each redox potential, absorption spectra were recorded between 575 and 540 nm wavelengths with a spatial resolution of 0.2 nm using a Jasco V550 spectrophotometer (Jasco, Groß-Umstadt, Germany) with a head-on photomultiplier. The monochromator slid width was set to 1 nm. Difference absorption spectra were deconvoluted, using reference spectra and difference extinction coefficients for the cytochromes as described [27]. PSII contents were calculated from the sum of the cyt-b_{559} HP and LP difference absorption signals [28].

PC and P_{700} redox kinetics and quantification - Difference absorption signals of PC and P_{700} were measured in the far-red range of the spectrum, essentially as described [29]. The contributions of PC and P_{700} were deconvoluted by measuring difference absorption changes at 830-870 nm (predominantly arising from P_{700}) and 870-950 nm (predominantly arising from PC). Measurements were done using a novel instrument developed in cooperation with C. Klughammer and U. Schreiber (in preparation). This instrument allows the simultaneous determination of both difference absorption signals. Measurements were done on pre-illuminated intact leaves with fully activated Calvin cycle, so that a limitation of P_{700} photooxidation by metabolic $NADP^+$ regeneration could be excluded. P_{700} and PC were photooxidized using far-red light (715 nm wavelength), which selectively excites PSI. After 10 s of far-red light, a saturating pulse of red light (6000 µE m^{-2} s^{-1}, 200 ms duration) was applied and the far-red light was switched off, so that PC and P_{700} could become fully reduced again after the end of the actinic light pulse. The reduction kinetics were fitted with a exponential function to determine the halftimes of PC and P_{700} reduction.

For PSI quantification in isolated thylakoids, membranes equivalent to 50 µg chl. ml^{-1} were solubilized in medium A (see above) containing 0.2% (w/v) DDM, 100 µM methylviologen as artificial electron acceptor and 10 mM ascorbate as electron donor. P_{700}, determined as described for measurements on intact leaves, was photooxidized by application of a saturating pulse of red light (6000 µE m^{-2} s^{-1} light intensity, 200 ms duration). For *in vitro* measurements of P_{700} and PC redox kinetics, 1 µM PC, isolated as described [29], together with 10 mM ascorbate and 100 µM tetramethyl-1.4-phenylendiamine (TMPD) were used as donor system.

Protein electrophoresis and immunoblotting - Thylakoid proteins were separated by SDS-polyacrylamide gel electrophoresis using a Perfect Blue twin gel system (PeqLab GmbH, Erlangen, Germany). Proteins were transferred to a PVDF membrane (Hybond P, Amersham Biosciences, Little Chelfont, UK) using a semidry blot system (SEDEC-M, PeqLab) and a standard transfer buffer (25 mM Tris, 192 mM glycine, pH 8.3). Immunoblot detection was done using the ECL system (Amersham Biosciences) according to the instructions of the manufacturer. Antibodies against Lhca1-4 and against Lhcb proteins were purchased from Agrisera AB (Vännäs, Sweden). All immunoblot data were confirmed for three independently grown batches of WT and mutant plants.

Results

Construction of *psaJ* knock-out mutants and isolation of homoplasmic lines - To facilitate the functional analysis of *psaJ* in higher plants, we constructed a *psaJ* knock-out by disrupting the reading frame with the selectable marker gene *aadA* (Fig. 1A). The *psaJ* knock-out allele was then introduced into the tobacco plastid genome by biolistic chloroplast transformation. Two homologous recombination events in the regions flanking the disrupted *psaJ* incorporate the knock-out allele into the plastid genome where it replaces the functional WT allele (Fig. 1A). Selection of bombarded leaf samples for resistance to spectinomycin conferred by the chimeric *aadA* marker gene yielded several transplastomic lines four of which were subjected to additional rounds of regeneration and selection to obtain homoplasmic tissue [21]. After three such rounds, plants were regenerated, rooted in sterile culture, subsequently transferred to soil and grown to maturity in the greenhouse. Seeds were obtained and analysis of the T1 generation by seed assays confirmed that the progeny was uniformly resistant to spectinomycin (data not shown). This suggested that the transformed chloroplast genome carrying the *psaJ*-disrupting *aadA* gene was present in a homoplasmic state and was inherited uniparentally maternally, as typical of a chloroplast-encoded trait [30]. All plants from all independently generated transplastomic lines were phenotypically identical (see below) and two independent lines (Nt-ΔpsaJ#9 and Nt-ΔpsaJ#20) were selected for further analysis. To verify homoplasmy moleculary and to confirm correct integration of the selectable marker gene *aadA* into the *psaJ* reading frame, RFLP assays (Fig. 1B) were performed. These experiments ultimately verified that the WT allele had been replaced by the knock-out allele in all copies of the chloroplast genome (Fig. 1B and data not shown). As all photosynthetic parameters (see below) of these two lines were highly similar, only average values for both lines will be presented.

Growth phenotype and functional organization of the photosynthetic apparatus in Δ*psaJ* plants - When grown under standard conditions for tobacco plants (600 µE m^{-2} s^{-1}, 16 h daylength), Δ*psaJ* plants did not display any visible phenotype (Fig. 1C). Growth, leaf size, number of leaves and flowering time were identical with WT plants (Fig. 1C). As some phenotypes of photosynthesis mutants become more pronounced with increasing leaf age, we determined all photosynthetic parameters for leaves of different ages from fully grown plants at the onset of flowering. As the youngest leaf, leaf number four (from the top of the plant) was analyzed, which was already largely expanded. In addition, leaves number six, nine and eleven were measured, with leaf number eleven being the oldest leaf not yet displaying any visible symptoms of senescence, although assimilation capacity (Fig. 2A) and chl. content (Fig. 2B) were already severely reduced. In both WT and Δ*psaJ* plants, chl. contents were highest in the youngest leaves (525 mg chl. m^{-2}), and decreased continuously with increasing leaf age to leaf number eleven, which contained only about 65% of the chl. content of leaf number four. No significant differences between the WT and Δ*psaJ* were observed (Fig. 2B).

However, interestingly, chl.-a/b ratios differed between WT and Δ*psaJ* plants (Fig. 2C): In Δ*psaJ* plants, the chl.-a/b ratio was slightly increased, the difference to the WT becoming more pronounced with increasing leaf age. Although such changes of the chl.-a/b ratio usually indicate alterations in the stoichiometries of the photosynthetic complexes, leaf assimilation capacities did not differ between the WT and the mutants (Fig. 2A): Again, the highest assimilation rates were obtained for the youngest leaves (about 600 µmoles electron pairs (EP) mg chl.$^{-1}$ h^{-1}), and declined to about half of the maximum assimilation capacity in the old leaves (275 µmoles EP mg chl.$^{-1}$ h^{-1}). These data already indicate that loss of PsaJ does not impair linear electron flux under saturating light intensities, suggesting that PsaJ is not essential for PSI assembly or function. To determine the molecular basis of the altered chl.-a/b ratios, we isolated thylakoids from the leaves used for the assimilation measurements. The contents of all redox-active proteins and protein complexes of the thylakoid membrane were determined by difference absorption spectroscopy and immunoblotting. The contents of PSII (Fig. 2D), cytochrome-bf-complex (cyt-bf) (Fig. 2E), and PSI (Fig. 2G), derived from difference absorption signals of cyt-b_{559} (PSII), cyt-b_6 and cyt-f (cyt-bf), and P_{700} (PSI), were determined in solubilized thylakoid membrane fragments. The PC contents, relative to P_{700}, were determined in intact leaves, and absolute PC contents were calculated based on the P_{700} quantification in solubilized thylakoids (Fig. 2F).

Significant differences between WT and Δ*psaJ* plants were obtained for the two photosystems: In WT plants, the PSI contents were about 2.3 mmoles PSI mol chl.$^{-1}$, independent of leaf age (Fig. 2G). In Δ*psaJ* knock-out plants, the PSI contents were significantly reduced already in leaf number four (approximately 80% of WT contents), and decreased further with increasing leaf age. In the oldest leaves, only about 70% of the PSI contents in the WT were detected. Conversely, PSII accumulated to slightly higher amounts in the Δ*psaJ* mutant than in the WT (Fig. 2D). Whereas young WT leaves contained about 3.0 mmoles PSII mol chl.$^{-1}$, mutant leaves contained 3.7 mmoles PSII mol chl.$^{-1}$. The increase in PSII contents in Δ*psaJ* may reflect a redistribution of chl. in favor of PSII due to the reduced PSI content, so that the relative proportion of PSII increases. With increasing leaf age and decreasing leaf assimilation capacity, a reduction of PSII contents was observed in both the WT and the mutant. For PC and cyt-bf contents (Figs. 2E and 2F), no significant differences between WT and Δ*psaJ* plants were detected. Both cyt-bf and PC accumulated to highest amounts in the youngest leaves, and decreased in parallel with assimilation capacity (Fig. 2A).

By and large, these spectroscopic quantifications were confirmed by immunoblot analyses using marker subunits of the photosynthetic complexes (Fig. 3). To test the dynamic range of the immunobiochemical detection reactions, a dilution series of the WT samples (100%, 50%, 20% and 10%) was used. Proteins from WT and *ΔpsaJ* leaves number four, six, nine and eleven were semiquantitatively analyzed by direct comparison with the dilution series. As a diagnostic subunit of PSII, the essential D2 protein encoded by *psbD* was used. Due to high sequence homology with the slightly smaller D1 protein (PsbA), a double band is always observed with our anti-D2 antibody. No obvious differences between the WT and the Δ*psaJ* mutant were observed with this antibody. This is

unsurprising, because the spectroscopic measurements provide a much more precise quantification of complex abundance and the slight increase in PSII contents in the mutant (Fig. 2D) was far too small to result in a visual quantitative effect in the immunoblot. For the cyt-bf, the essential subunit cyt-f (PetA) was used as a diagnostic subunit [31]. Here, the about 50% decrease of cyt-bf content with increasing leaf age is clearly visible. For the PsaC protein, which binds the stromal iron-sulfur clusters of PSI and is essential for PSI accumulation [5], the signals obtained in the mutants are slightly weaker than in the WT. However, the measured 20-30% lower PSI amounts in the mutant are at the borderline of detectability with immunoblotting techniques and the spectroscopic data provide a much more reliable dataset here. A strong leaf-age dependent decrease was observed for the marker subunit of the ATP synthase, AtpA, both in the WT and the mutant. The weak lower band results from a cross-reaction of our antibody with the AtpB subunit, which shares some sequence similarity with AtpA. In essence, within the detection limits of immunoblots (which are only semiquantitative), the spectroscopic results were confirmed.

PSI stability and function - To determine if the reduced PSI contents in the Δ*psaJ* mutants (Fig. 2G) can be attributed to a reduced stability of PSI in the absence of its J-subunit, WT and mutant plants were subjected to stress treatments that potentially affect PSI. To assess PSI stability *in vivo*, tobacco plants were subjected to chilling stress. Plants were transferred to 4°C and 100 $\mu E\ m^{-2}\ s^{-1}$ light intensity. These conditions have been described to selectively damage PSI, due to inhibition of the Mehler-Asada cycle and accumulation of reactive oxygen species on the PSI acceptor side. In *Arabidopsis* and barley, a few hours of cold stress were sufficient to result in the loss of up to 50% of PSI [32,33]. Surprisingly, short term cold stress of up to 24 h had no effect on the amount of redox-active PSI and on assimilation (data not shown). PSI damage was detectable only after several days of chilling stress, but no differences could be observed between the WT and the Δ*psaJ* mutant (not shown). Apparently, tobacco is far more tolerant to cold stress than *Arabidopsis thaliana* and barley.

Additional treatments that potentially destabilize PSI were performed *in vitro* using isolated thylakoids, which were subjected to repetitive cycles of freezing and thawing, to heat stress (10 min incubation at 70°C) or to incubation in chaotropic salt solutions. Afterwards, thylakoids were partly solubilized by addition of 0.2% (w/v) β-dodecyl-maltoside (DDM) to optimize the optical properties of the sample. Ascorbate was used as electron donor to keep P_{700} reduced in darkness. Methylviologen functioned as electron acceptor during photooxidation. Up to 15 cycles of repetitive freezing in liquid nitrogen and thawing at 35°C had no significant effect on the amplitude of the P_{700} difference absorption signal (Fig. 4A). In response to heat stress (10 min incubation at 70° C), a 20% reduction in the maximum amplitude of P_{700} became apparent. However, no difference between the WT and the Δ*psaJ* mutant was observed. Also, 10 min incubation with different chaotropic reagents did not result in significantly different effects on the maximum oxidizable fraction of P_{700} in the WT and the mutant. Both 2 M KI and 2 M NaBr resulted in some reduction of the P_{700} amplitude, the effect being slightly more pronounced in mutant thylakoids. Due to high standard deviations, these differences are not

statistically significant. Evidently, the J-subunit is not required to stabilize the intra-complex electron transfer from P_{700} to the artificial acceptor methylviologen.

However, interestingly, solubilization of PSI with 0.2 % (w/v) DDM resulted in a clearly delayed P_{700} reduction in the Δ*psaJ* mutant after the end of the saturating light pulse (not shown). To analyze this effect in more detail, and to exclude that different reduction kinetics of WT and mutant PSI might be due to different PC contents still associated with PSI after solubilization, P_{700} redox kinetics of solubilized PSI particles were measured in the presence of 1 µM PC, with 10 mM ascorbate and 100 µM TMPD as electron donors to PC (Fig. 4B). In the WT, almost 85% of P_{700} were reduced with a halftime of less than 8 ms by PC. Only a small fraction of approximately 15% of PSI displayed an extremely slow reduction (halftime > 500 ms). As the relative proportion of this fraction was independent of PC contents added to the sample, we conclude that this fraction represents PSI with damaged donor side, which cannot bind PC efficiently anymore. In the Δ*psaJ* mutant, the slow fraction was much larger with 50% of PSI being inefficiently reduced (Fig. 4B). Therefore, in the Δ*psaJ* mutant, the PSI donor side seems to be much more prone to damage or suffers from aberrant conformational changes, comparable to the situation in a *Chlamydomonas psaJ* mutant, where *in vitro* PSI redox kinetics also revealed a large fraction of P_{700} not being efficiently reduced by PC or cytochrome c [13]. To test whether defects in PC-P_{700} interaction are also observable *in vivo*, a detailed analysis of the redox equilibration between PC and P_{700} was conducted on intact leaves.

Redox equilibration of PC and P_{700} - To analyze the *in vivo* redox equilibration of PC and P_{700}, intact leaves were pre-illuminated to fully activate the Calvin cycle and avoid an acceptor side limitation of P_{700}. Complete photooxidation of the "high-potential chain" comprising cyt-f, PC and P_{700} and complete photoreduction of the plastoquinone (PQ) pool was achieved by applying an over-saturating light pulse (6000 µE m^{-2} s^{-1}, 200 ms duration). After the flash, both the over-saturating light pulse and the actinic illumination were switched off (time point 0 in Fig. 5A), and the reduction of PC and P_{700} by electrons from the PQ pool was determined. In Fig. 5A, exemplary kinetics of PC and P_{700} reduction measured in young leaves are shown. The fully oxidized states of PC and P_{700} at the end of the light pulse were normalized to one, the completely reduced states were normalized to zero. Reduction halftimes of P_{700} of approximately 3.5 ms were obtained, without any significant differences between WT and the Δ*psaJ* mutant (Fig. 5A). With increasing leaf age, the reduction halftime of P_{700} increased in both WT and mutant plants to about 10 ms (data not shown), which reflects the about 50% reduction in assimilation capacity of older leaves (cp. Fig. 2A). In accordance with the higher redox potential of P_{700}, electrons accumulated in the PC pool only when the majority of P_{700} was reduced. No significant differences between the WT and the Δ*psaJ* mutant were observed (Fig. 5A). Although the PC and P_{700} reduction kinetics normally are limited by PQ re-oxidation at cyt-bf, a severe disturbance of the interaction between PC and P_{700} as observed in the mutant *in vitro* (Fig. 4B), is expected to result in a visible delay of net P_{700} reduction and an accelerated electron accumulation at PC. This was not observed, strongly arguing against a role of PsaJ in PC oxidation in

higher plants. To test for subtle changes in the interaction between PC and P_{700}, the reduction kinetics of both components were plotted against each other (Fig. 5B), and the apparent redox equilibration constants (k_{app}) were calculated [29]. K_{app} values in the range of 5 to 12 were obtained. On average, both the WT and the Δ*psaJ* mutants had a k_{app} of 7.5. Thus, neither redox kinetics nor redox equilibration between PC and P_{700} are affected by PsaJ under physiological conditions in tobacco.

Antenna analysis - In addition to its close vicinity to the PC binding site, PsaJ is also part of the interface of PSI with the Lhca antenna proteins and has been hypothesized to be involved in exciton transfer from the antenna to the PSI reaction center [16]. To address the possible role of PsaJ in exciton transfer from the peripheral antenna to the PSI reaction center, light saturation curves of linear electron flux were measured. Under low light intensities, the quantum efficiency of PSII was found to be significantly lower in the Δ*psaJ* mutant than in the WT. Also, the PQ pool was considerably more reduced in the mutant, as concluded from significantly increased (1-qL) values (Fig. 6A). With increasing light intensity, this difference between the Δ*psaJ* mutant and the WT decreased progressively and eventually disappeared above 600 µE m^{-2} s^{-1} light intensity (Fig. 6A). This suggests that exciton transfer to P_{700} is less efficient in the mutant, so that PSI excitation limits linear electron flux and assimilation under low light intensities. Indeed, when plants were grown under low-light conditions (two weeks at 20 µE m^{-2} s^{-1}), Δ*psaJ* transformants developed a clearly discernable mutant phenotype. Growth was retarded and the chl. content per leaf area was visibly reduced (Fig. 6B). When plants were transferred back to standard light intensities (600 µE m^{-2} s^{-1}), these phenotypic differences disappeared.

PSI antenna organization and antenna function of plants grown under standard light conditions was further analyzed using Lhc isoform-specific antibodies (Fig. 7) and performing 77 K chl.-a fluorescence emission measurements (Fig. 8). Similar to the quantification of the photosynthetic complexes (Fig. 3), thylakoids isolated from leaves number four, six, nine and eleven were used for immunoblot analyses of antenna protein accumulation. For the Lhcb proteins, no significant differences between WT and Δ*psaJ* plants were observed (Fig. 7). In contrast, analysis of Lhca accumulation revealed a specific depletion of Lhca3 in Δ*psaJ* plants, whereas the other Lhca isoforms accumulated to approximately the same amounts as in WT thylakoids. Specific changes in the functional organization of the PSI antenna system are further supported by 77 K chl.-a fluorescence emission analysis (Fig. 8): 77 K fluorescence emission spectra of WT and Δ*psaJ* thylakoids were normalized to the PSII emission maximum at 686 nm wavelength, since no differences in PSII fluorescence emission properties were expected to occur in the Δ*psaJ* mutants. Indeed, the low-wavelength part of the fluorescence emission spectrum, which arises from PSII and LHCII fluorescence, was unaltered in Δ*psaJ* thylakoids compared to the WT. However, the far-red emission maximum of the PSI-LHCI system was clearly blue-shifted in the Δ*psaJ* mutant. Whereas for WT thylakoids, a typical emission peak at 733 nm was observed, in agreement with previously obtained 77 K emission spectra of tobacco [34], the maximum emission of the Δ*psaJ* mutant was shifted to 728 nm

(Fig. 8). This blue-shift of chl.-a fluorescence emission was observed in all leaves of the mutant, independent of their ontogenetic state (not shown). Also, the overall fluorescence emission from the PSI-LHCI system relative to PSII was reduced in the mutant, which is in good agreement with the decreased PSI contents and the slight complementary increase in PSII contents (see Fig. 2).

To test whether the loss of PsaJ also interferes with the capacity of PSI to bind LHCII, state transitions were induced by blue light-enriched illumination of young leaves to reduce the PQ pool and induce antenna redistribution in favor of PSI (state 2). Subsequently, the PQ pool was reoxidized by far-red light-enriched illumination inducing return to state 1. When the amplitudes of state transitions were calculated [26], no significant differences between the WT (F_T = 0.85, SD = 0.14) and the Δ*psaJ* mutant (F_T = 0.72, SD = 0.16) were found, suggesting that PsaJ is not required for LHCII binding to PSI.

Discussion

Today, the overall function of higher plant PSI is quite well understood, mainly due to the availability of a crystal structure from pea [3] and the characterization of knock-out or antisense/RNAi mutants lacking specific nuclear-encoded subunits [6,7]. A notable exception is the limited knowledge about the role of the small plastome-encoded I- and J-subunits of PSI, whose functions have not yet been resolved in higher plants. This is because the generation of plants with transgenic chloroplasts is still significantly more challenging than nuclear transformation [19,20]. The PsaJ subunit is particularly interesting, because, based on the available crystal structural data, a dual function has been proposed: In view of its localization in close vicinity to both the LHCI and the PC binding sites, involvement in both PSI excitation and donor side reactions has been discussed. Furthermore, the plastid localization of the *psaJ* gene was considered to indicate an important function of this small subunit, as the other plastome-encoded PSI subunits, PsaA, PsaB and PsaC, have all been proven to be essential for PSI biogenesis in eukaryotes, whereas the vast majority of the nuclear-encoded subunits is not [7]. However, a comparable suggestion has recently been proven wrong for the cyt-bf, as deletion of the plastid-encoded PetL subunit does not result in a visible phenotype [35]. Therefore, the assumption that deletion of plastid-encoded subunits of photosynthetic complexes should result in stronger phenotypes than deletion of nuclear-encoded subunits is not necessarily correct.

The function of the J-subunit has been investigated previously in *Chlamydomonas*. Here, a role in the conformational stabilization of the PC-binding site has been identified [13]. Surprisingly, although the impaired PC binding by PSI should be expected to result in a growth phenotype, this was not observed [13]. PSI contents in the *Chlamydomonas* Δ*psaJ* mutants were normal, and the role of PsaJ in exciton transfer to the PSI reaction center was not addressed. In view of these unresolved

issues and existing evidence that the functions of photosynthetic proteins can vary considerably between *Chlamydomonas* and higher plants [31], we addressed the functions of PsaJ in tobacco.

In this work, we have successfully generated homoplasmic knock-out transformants by disrupting the *psaJ* reading frame with the *aadA* antibiotic resistance marker. Our finding that, when grown at standard growth conditions, the knock-out lines do not display a visible phenotype, clearly demonstrates that PsaJ is not essential for PSI accumulation and function. The absence of a discernable phenotype is in agreement with the unaltered chl. contents per leaf area and the identical assimilation capacities of WT and knock-out plants (Fig. 2), and is reminiscent of the situation in *Chlamydomonas*. However, different from *Chlamydomonas*, loss of PsaJ resulted in a 20 to 30% reduction of PSI contents in tobacco which was slightly more pronounced in older leaves (Fig. 2). More importantly, loss of PsaJ had no influence on *in vivo* PC-P_{700} interactions and redox equilibration in tobacco (Fig. 5). Thus, PsaJ is obviously not required for the stabilization of the PC-binding site *in vivo*. However, in response to thylakoid solubilization, the reduction of PSI by PC was impaired in the mutant, whereas the same treatment had no effect on the P_{700} reduction kinetics in the WT. This *in vitro* phenotype closely resembles that of *Chlamydomonas* PsaJ knock-out mutants, where the fast reduction of PSI by either PC or cyt-c_6 was almost completely abolished [13]. This may indicate that also in higher plants, PsaJ can help stabilizing the PC-binding site. However, this aspect of PsaJ function seems to become relevant only under non-physiological conditions *in vitro*. It is noteworthy in this respect, that the PC-P_{700} interaction studies in *Chlamydomonas reinhardtii* were done using isolated PSI particles, so that, potentially, the observed effects could also have been caused by the *in vitro* conditions. Remarkably, no effect of the PsaJ deletion on overall growth of *Chlamydomonas* was reported [13], which might indicate that the observed strong effect on PC oxidation may occur only *in vitro*, as demonstrated here for tobacco.

Whereas the role of PsaJ for PSI stability and PC oxidation seems to be of only limited importance in higher plants, our data strongly suggest that its predominant function resides in PSI excitation. This conclusion is supported by several lines of evidence. First, the growth of the Δ*psaJ* mutant is retarded under low light conditions, whereas no phenotype is seen at higher growth light intensities (Figs. 1C and 6B). Second, the PQ pool is more reduced in low light in the mutant than in the WT (Fig. 6A). Third, the 77 K chl.-a fluorescence emission spectrum of the PSI-LHCI complex is blue-shifted (Fig. 8). Finally, the accumulation of Lhca proteins is altered in the mutant (Fig. 7). Together, these results support a scenario, in which PsaJ functions in LHCI binding and exciton transfer to the PSI reaction center, thereby enlarging the functional PSI antenna cross section. In the absence of PsaJ, PSI excitation seems to be less efficient, either due to uncoupling of LHCI from PSI or as a consequence of impaired exciton transfer from LHCI to the reaction center, for which the two chl.-a molecules bound to PsaJ could be required. The reduced efficiency of PSI excitation results in an imbalance between PSI and PSII excitation in low light and a more reduced redox state of the PQ pool at limiting light intensities. Surprisingly, the mutants are not capable of compensating for this

imbalance in photosystem excitation, although their capacity for state transitions was found to be normal. Therefore, the PSI-oxidizing capacity seems to limit linear electron flux in low light. Under high light intensities, both the growth phenotype and the more reduced redox state of the mutant's PQ pool disappear, because now photosystem excitation is no longer limiting, but instead, linear electron flux itself becomes limiting for assimilation and growth.

The exact molecular basis of the altered antenna function in Δ*psaJ* plants is currently difficult to elucidate: Crystal structures indicate that PsaJ is most likely located in direct vicinity of Lhca2 [3,16]. However, due to the high homology between Lhca2 and Lhca3, the attribution of the protein structure closest to PsaJ to Lhca2 is not unequivocal [36]. Interestingly, our immunoblot analyses revealed that Lhca2 contents remain unaltered in the mutant, while Lhca3 levels are significantly reduced in the knock-out plants. Also, the 77 K chl.-a fluorescence emission data may be easier to reconcile with a predominant effect on Lhca3 accumulation and function than with an effect on Lhca2: At least *in vitro*, the Lhca2 chl.-a fluorescence emission peaks at 701 nm wavelength [37,38] and thus in the part of the fluorescence spectrum which is still very similar to the WT spectrum (Fig. 8). Only in the wavelength range above 700 nm, clear differences between Δ*psaJ* and WT thylakoids become apparent: Difference spectra of WT minus *ΔpsaJ* mutant revealed a negative peak at 715 nm and a positive peak at 735 nm (not shown). The predominant contribution to *in vitro* 77 K fluorescence emission in this spectral range arises from Lhca3 and Lhca4 [37,38]. Although *in vitro* emission from the *Arabidopsis* Lhca3 isoform is maximal at 725 nm [37], *in vivo* data suggest that Lhca3 may emit predominantly in the 730 nm range, most likely due to interaction effects with the PSI reaction center and the other Lhca proteins. Significantly, Lhca3 antisense plants revealed a reduced and slightly blue-shifted 77 K fluorescence emission, comparable to the effects observed in our Δ*psaJ* transformants [39]. Most importantly, the difference spectra between the WT and the Lhca3 antisense plants [39] are practically identical with those obtained here for WT and Δ*psaJ* plants. Thus, the observed 77 K spectra are in excellent agreement with the selective reduction of Lhca3 revealed by immunoblots. Taken together, these data support the suggestion that the Lhca protein localized in direct vicinity of PsaJ is not Lhca2, but rather Lhca3 [36].

Interestingly, an effect of PSI subunit deletion on the accumulation of antenna proteins has been reported also for other small subunits of the complex. For example, *psaK* antisense and T-DNA insertion mutants in *Arabidopsis* [12,40] display a reduced accumulation of Lhca3. However, in both PsaK mutants and Lhca3 antisense plants [39], loss or reduced accumulation of Lhca3 results in a concomitant reduction in Lhca2 accumulation, which is most readily explained with a close physical interaction between Lhca2 and Lhca3 [41]. Our Δ*psaJ* mutant is unique in that this concomitant reduction in Lhca2 does not occur. The structural basis for this observation remains to be determined.

Another interesting question concerns the molecular cause of the reduced PSI contents in the Δ*psaJ* mutant. In theory, this could be either due to a slightly less efficient assembly of PSI or to an accelerated degradation. The latter effect could result from a subtle general destabilization of PSI

subunit interactions in the absence of PsaJ. Alternatively, in the absence of its J-subunit, the PSI complex could be more accessible to proteolytic breakdown, for example, due to increased exposure of protease-susceptible domains at its surface. Our *in vitro* measurements of PSI stability in response to repetitive freezing and thawing, heat stress and treatments with chaotropic reagents (Fig. 4A) argue against a general destabilization of protein-protein interactions within the complex in the absence of PsaJ, as none of these treatments resulted in an accelerated loss of redox-active PSI. Although the PC-binding site may be bound slightly less tightly, our redox equilibration measurements indicate that this effect is not relevant under physiological conditions (Fig. 5). Therefore, a scenario, in which PSI without PsaJ is more prone to proteolytic degradation may seem more likely. However, as no PSI-degrading proteolytic activity has been characterized to date [42], it is currently not possible to test for an increased accessibility of PSI to native thylakoid proteases.

Finally, our finding that maximum assimilation rates in Δ*psaJ* are identical with those in the WT, despite of a 20% reduction in PSI accumulation, represents a potentially important observation. It implies that PSI, at least in WT plants, does not contribute to photosynthetic flux control. Instead, flux control is exerted at the level of the cyt-bf (Fig. 2E), in agreement with previous data [43,44]. Potentially, also PC could contribute (Fig. 2F), as its contents decrease in parallel with cyt-bf content and assimilation capacity [24]. As the PsaJ mutant plants, despite a 20% reduction of PSI contents, can support the same maximum assimilation rates as the WT, it seems clear that plants possess an overcapacity of PSI. This overcapacity may be even greater than revealed by the Δ*psaJ* mutant, because cyt-bf accumulates to far lower levels than PSI (1.5 mmoles cyt-bf mol chl.$^{-1}$ versus 2.3 mmoles PSI mol chl.$^{-1}$). The halftime of PQ reoxidation, the rate-limiting reaction at the cyt-bf, is in the range of 2 to 3 ms [45], and therefore several times slower than PC oxidation by P_{700} and electron transfer through the PSI complex to ferredoxin, which overall requires less than 1 ms. From these values, a several-fold potential overcapacity of PSI, relative to linear electron flux, can be expected, and therefore, the absence of any effect of the diminished PSI contents in Δ*psaJ* plants on overall assimilation is unsurprising. Currently, it is not understood why higher plants accumulate much higher PSI contents than theoretically necessary to support electron flux. One plausible explanation could be, that under certain environmental conditions, a high number of PSI complexes is beneficial to compensate for the low-affinity PC binding [46] and/or the inefficient unbinding of PC from PSI [46]. However, a rigorous analysis of the physiological functions of the PSI overcapacity will require modulation of PSI levels without altering PSI subunit composition.

Acknowledgements: We thank Britta Hausmann for plant cultivation and Dr. Stefanie Hartmann for help with vector construction. This project was supported by a grant of the Deutsche Forschungsgemeinschaft to M.A.S. and R.B. (SFB 429, project A12) and by the Max Planck Society.

Literature cited

1 Khrouchtchova, A., Hansson, M., Paakkarinen, V., Vainonen, J.P., Zhang, S., Jensen, P.E., Scheller, H.V., Vener, A.V., Aro, E.M. and Haldrup, A. (2005) A previously found thylakoid membrane protein of 14kDa (TMP14) is a novel subunit of plant photosystem I and is designated PSI-P. FEBS Lett. **579,** 4808-4812

2 Ganeteg, U., Klimmek, F. and Jansson, S. (2005) Lhca5 – an LHC-type protein associated with photosystem I. Plant Mol. Biol. **54,** 641-651

3 Ben-Shem, A., Frolow, F. and Nelson, N. (2003) The crystal structure of plant photosystem I. Nature **426,** 630-635

4 Takahashi, Y., Goldschidt-Clermont, M., Soen, S.Y., Franzen, L.G. and Rochaix, J.D. (1991) Directed chloroplast transformation in *Chlamydomonas reinhardtii*: insertional inactivation of the psaC gene encoding the iron sulfur protein destabilises photosystem I. EMBO J. **10,** 2033-2040

5 Wostrikoff, K., Girard-Bascou, J., Wollman, F.A. and Choquet, Y. (2004) Biogenesis of PSI involves a cascade of translational autoregulation in the chloroplast of Chlamydomonas. EMBO J. **23,** 2696-2705

6 Scheller, H.V., Jensen, P.E., Haldrup, A., Lunde, C. and Knoetzel, J. (2001) Role of subunits in eukaryotic photosystem I. Biochim. Biophys. Acta **1507,** 41-60

7 Jensen, P.E., Haldrup, A., Rosgaard, L. and Scheller, H.V. (2003) Molecular dissection ofphotosystem I in higher plants: topology, structure and function. Physiol. Plant. **119,** 313-321

8 Ihnatowicz, A., Pesaresi, P., Varotto, C., Richly, E., Scheider, A., Jahns, P., Salamini, F. and Leister, D. (2004) Mutants of photosystem I subunit D of Arabidopsis thaliana: effects on photosynthesis, photosystem I stability and expression of nuclear genes for chloroplast functions. Plant J. **37,** 839-852

9 Haldrup, A., Lunde, C. and Scheller, H.V. (2003) Arabidopsis thaliana plants lacking the PSI-D subunit of photosystem I suffer severe photoinhibition, have unstable photosystem I complexes, and altered redox homeostasis in the chloroplast stroma. J. Biol. Chem. **278,** 33276-33283

10 Ihalainen, J.A., Jensen, P.E., Haldrup, A., van Stokkum, I.H.M., van Grondelle, R., Scheller, H.V. and Dekker, J.P. (2002) Pigment organization and energy transfer dynamics in isolated photosystem I (PSI) complexes from Arabidopsis thaliana depleted of the PSI-G, PSI-K, PSI-L, or PSI-N subunit. Biophysical J. **83,** 2190-2201

11 Jensen, P.E., Haldrup, A., Zhang, S. and Scheller, H.V. (2004) The PSI-O subunit of plant photosystem I is involved in balancing the excitation pressure between the two photosystems. J. Biol. Chem. **279,** 24212-24217

12 Varotto, C., Pesaresi, P., Jahns, P., Leßnick, A., Tizzano, M., Schiavon, F., Salamini, F. and Leister, D. (2002) Single and double knockouts of the genes for photosystem I subunits G, K and H of Arabidopsis. Effect on photosystem composition, photosynthetic electron flow, and state transitions. Plant Physiol. **129,** 616-624

13 Fischer, N., Boudreau, E., Hippler, M., Drepper, F., Haehnel, W. and Rochaix, J.D. (1999) A large fraction of PsaF is nonfunctional in photosystem I complexes lacking the PsaJ subunit. Biochemistry **38,** 5546-5552

14 Chitnis, P.R. (1996) Photosystem I. Plant Physiol. **111,** 661-669

15 Xu, Q., Odom, W.R., Guikema, J.A., Chitnis, V.P. and Chitnis, P.R. (1994) Targeted deletion of PsaJ from the cyanobacterium Synechocystis SP PCC-6803 indicates structural interactions between the PsaJ and PsaF subunits of photosystem-I. Plant Mol. Biol. **26,** 291-302

16 Ben-Shem, A., Frolow, F. and Nelson, N. (2004) Light harvesting features revealed by the structure of plant photosystem I. Photosynth. Res. **81,** 239-250

17 Ruf, S., Kössel, H. and Bock, R. (1997) Targeted inactivation of a tobacco intron containing open reading frame reveals a novel chloroplast-encoded photosystem I-related gene. J. Cell Biol. **139,** 95-102

18 Hager, M., Biehler, K., Illerhaus, J., Ruf, S. and Bock, R. (1999) Targeted inactivation of the smallest plastid-genome encoded open reading frame reveals a novel and essential subunit of the cytochrome-b(6)complex. EMBO J. **18,** 5834-5842

19 Maliga, P. (2004) Plastid transformation in higher plants. Annu. Rev. Plant. Biol.. **55,** 289-313

20 Bock, R. and Khan, M.S. (2004) Taming plastids for a green future. Trends Biotechnol. **22,** 311-318

21 Svab, Z. and Maliga, P. (1993) High frequency plastid transformation in tobacco by selection for a chimceric *aadA* gene. Proc. Natl. Acad. Sci. USA **90,** 913-917

22 Porra, R.J., Thompson, W.A. and Kriedermann, P.E. (1989) Determination of accurate extinction coeffiicent and simultaneous equations for essaying chlorophylls a and b extracted with four different solvents: verification of the concentration of chlorophyll standards by atomic absorption spectroscopy. Biochim. Biophys. Acta **975,** 384-394

23 Raghavendra, A.S. and Padmasree, K. (2003) Beneficial interactions of mitochondrial metabolism with photosynthetic carbon assimilation. Trends Plant Sci. **8,** 546-553

24 Schöttler, M.A., Kirchhoff, H. and Weis, E. (2004) The role of plastocyanin in the adjustment of photosynthetic electron transport to the carbon metabolism in tobacco. Plant Physiol **136,** 4265-4274

25 Kramer, D.M., Johnson, G., Kiirats, O. and Edwards, G.E. (2004) New fluorescence parameters for the determination of Q(A) redox state excitation energy fluxes. Photosynth. Res. **79,** 209-218

26 Lunde, C., Jensen, P.E., Haldrup, A., Knoetzel, J. and Scheller, H.V. (2000) The PSI-H subunit of photosystem I is essential for state transitions in plant photosynthesis. Nature **408,** 613-615

27 Kirchhoff, H., Mukherjee, U. and Galla, H.J. (2002) Molecular architecture of the thylakoid membrane: Lipid diffusion space for plastoquinone. Biochemistry **41,** 4872-4882

28 Lamkemeyer, P., Laxa, M., Collin, V., Li, W., Finkemeyer, I., Schottler, M.A., Holtkamp, V., Tognetti, V.B., Issakidis-Bourguet, E., Kandlbinder, A., Weis, E., Miginiac-Maslow, M. and Dietz, K.J. (2006) Peroxiredoxin Q of Arabidopsis thaliana is attached to the thylakoids and functions in context of photosynthesis. Plant J. **45,** 968-981

29 Kirchhoff, H., Schöttler, M.A., Maurer, J. and Weis, E. (2004) Plastocyanin redox kinetics in spinach chloroplasts: evidence for disequilibrium in the high potential chain. Biochim. Biophys. Acta **1659,** 63-72

30 Bock, R. (2001) Transgenic plastids in basic research and plant biotechnology. J. Mol. Biol. **312,** 425-438

31 Monde, R.A., Zito, F., Olive, J., Wollman, F.A. and Stern, D.B. (2000) Post-transcriptional defects of tobacco chloroplast mutants lacking the cytochrome-bf complex. Plant J. **21,** 61-72

32 Zhang, S. and Scheller, H.V. (2004) Photoinhibition of photosystem I at chilling temperature and subsequent recovery in Arabidopsis thaliana. Plant Cell Physiol. **45,** 1595-1602

33 Scheller, H.V. and Haldrup, A. (2005) Photoinibition of photosystem I. Planta **221,** 5-8

34 Bondarava, N., De Pascalis, L., Al-Babili, S., Goussias, C., Golecki, J.R., Beyer, P., Bock, R. and Krieger-Liszkay, A. (2003) Evidence that cytochrome b_{559} mediates the oxidation of reduced plastoquinone in the dark. J Biol. Chem. **278,** 13554-13560

35 Fiebig, A., Stegemann, S. and Bock, R. (2004) Rapid evolution of RNA editing sites in a small non-essential plastid gene. Nucleic Acids Res. **32,** 3615-3622

36 Jolley, C., Ben-Shem, A., Nelson, N. and Fromme, P. (2005) Structure of plant photosystem I revealed by theoretical modeling. J. Biol. Chem. **280,** 33627-33636

37 Castelletti, S., Morosinotto, T., Robert, B., Caffarri, S., Bassi, R. and Croce, R. (2003) Recombinant Lhca2 and Lhca3 subunits of the photosystem I antenna system. Biochemistry **42,** 4226-4234

38 Croce, R., Morosinotto, T., Ihalainen, J.A., Chojnicka, A., Breton, J., Dekker, J.P., van Grondelle, R. and Bassi, R. (2004) Origin of the 701nm fluorescence emission of the Lhca2 subunit of higher plant photosystem I. J. Biol. Chem. **279,** 48543-48549

39 Ganeteg, U., Strand, A., Gustafsson, P. and Jansson, S. (2001) The properties of the chlorophyll a/b-binding proteins Lhca2 and Lhca3 studied in vivo using antisense inhibition. Plant Physiol. **127,** 150-158

40 Jensen, P.E., Gilpin, M., Knoetzel, J. and Scheller, H.V. (2000) The PSI-K subunit of photosystem I is involved in the interaction between light-harvesting complex I and the photosystem I reaction center core. J. Biol. Chem. **275,** 24701-24708

41 Jansson, S., Andersen, B. and Scheller, H.V. (1996) Nearest-neighbor analysis of higher-plant photosystem I holocomplex. Plant Physiol. **112,** 409-420

42 Adam, Z., Rudella, A. and van Wijk, K.J. (2006) Recent advances in the study of Clp, FtsH and other proteases located in chloroplasts. Curr. Opin. Plant Biol. **9,** 234-240

43 Anderson, J.M. (1992) Cytochrome-bf complex: Dynamic molecular organization, function and acclimation. Photosynth. Res. **34,** 341-357

44 Anderson, J.M., Price, G.D., Chow, W.S., Hope, A.B. and Badger, M.R. (1997) Reduced levels of cytochrome bf complex in transgenic tobacco leads to a marked photochemical reduction of the plastoquinone pool, without significant change in acclimation to irradiance. Photosynth. Res. **53,** 215-227

45 Hope, A.B. (2000) Electron transfers amongst cytochrome f, plastocyanin and photosystem I: kinetics and mechanisms. Biochim. Biophys. Acta **1456,** 5-26

46 Finazzi, G., Sommer, F. and Hippler, M. (2005) Release of oxidised plastocyanin from photosystem I limits electron transfer between photosystem I and cytochrome b6f complex in vivo. Proc. Natl. Acad. Sci. USA **102,** 7031-7036

Figure legends:

Figure 1. Generation of *psaJ* knock-out plants. (A) Construction of a *psaJ* null allele by disruption with the *aadA* selection marker. Physical maps of the *psaJ* region in the WT plastid genome and the plastome in Δ*psaJ* plants are depicted. Genes above the line are transcribed from the left to the right, genes below the line are transcribed in the opposite direction. Relevant restriction sites used for cloning and RFLP analysis are indicated. Sites lost due to ligation to heterologous ends are shown in parentheses. (B) RFLP analysis to confirm homoplasmy and *psaJ* disruption by the chimeric *aadA* cassette. DNA samples were digested with the restriction enzyme SalI which produces a 5.5 kb fragment for the *psaJ* region in the WT (see part A). Disruption of the *psaJ* gene with the *aadA* selection marker results in a size increase of the probed restriction fragment by 1.1 kb. As expected, Southern blot analysis (probed with a radiolabeled PCR product covering the entire *psaJ* coding region) confirms the absence of the smaller 5.5 kb WT fragment from the transplastomic lines demonstrating that they are homoplasmic. (C) Phenotypic comparison of WT and Δ*psaJ* plants under standard growth conditions. The transplastomic knockout lines do not show any visible phenotype when grown in a controlled environment chamber under a light intensity of 600 $\mu E\ m^{-2}\ s^{-1}$.

Figure 2. Assimilation capacities and chl. contents are unaltered, but the chl.-a/b ratio and photosystem accumulation are altered in Δ*psaJ* plants. The first fully expanded leaf (number four from the top) and leaves number six, nine and eleven were comparatively analyzed to determine possible phenotypic alterations arising during leaf ontogenesis. Data for the WT are presented as filled circles, data for the Δ*psaJ* mutant (PsaJ) are indicated as open circles. Leaf assimilation capacities of WT and Δ*psaJ* mutants are identical (A). No effect on the chl. content per leaf area is observed (B), but the chl.-a/b ratio is slightly elevated in the Δ*psaJ* mutant (C), indicating some changes in thylakoid complex stoichiometries. Thylakoids were isolated from the leaves measured to obtain the data sets displayed in Fig. 2D-G. Photosystem contents were determined from cyt-b_{559} (PSII) and P_{700} (PSI) difference absorption signals, respectively. Cyt-bf quantification was based on difference absorption signals of cyt-f and cyt-b_6, PC was measured in the far-red range of the spectrum. In the Δ*psaJ* mutant, PSII contents (D) are significantly increased, probably as a consequence of reduced PSI accumulation (G). No differences between mutant and WT were observed for cyt-bf (E) and PC contents (F), which both correlate closely with assimilation capacities (A).

Figure 3. Immunoblot analysis of marker proteins for the four multisubunit complexes of the photosynthetic light reactions. PsbD (D2-protein) is an essential component of the PSII reaction center. PetA (cyt-f) is essential for cyt-bf accumulation. PsaC is part of the PSI reaction center and required for biogenesis and stability of the PSI complex. AtpA is an essential component of the chloroplast ATP synthase. The first four lanes of each blot show undiluted thylakoids from WT leaves

(leaf number 4) and a dilution series (50%, 20% and 10% of the undiluted sample) to determine the response range of the antibody. The next four lanes display WT thylakoids isolated from leaves number four (lane 5), six (lane 6), nine (lane 7) and eleven (lane 8). Lanes nine to twelve show thylakoids isolated from the corresponding mutant leaves. Double signals for PsbD arise from cross-reactions with the homologous D1 protein; cross reactions of the AtpA antibody are due to hybridization with the slightly smaller AtpB subunit.

Figure 4. Overall stability of P_{700} in response to stress treatments is unaltered in Δ*psaJ* thylakoids (A), but the PSI donor side is more prone to damage (B). Thylakoids isolated from young WT and Δ*psaJ* (PsaJ) leaves were subjected to 15 repetitive cycles of freezing in liquid nitrogen and thawing at 35°C, to heating to 70° C for 10 min, and to 10 min incubation with chaotropic salts (1 M NaCl, 2 M KI, 2 M NaBr). Afterwards, the maximum amplitude of photooxidizable P_{700} was determined by difference absorption spectroscopy. None of the treatments resulted in selective destabilization of the mutant PSI complex. Heating to 70°C resulted in loss of about 25% of PSI in both WT and the Δ*psaJ* mutant, the other treatments had even smaller effects on the P_{700} amplitude. However, *in vitro* P_{700} redox kinetics of detergent-solubilized thylakoids reveal an impaired P_{700} photoreduction in Δ*psaJ* mutants (B). The reduced state of P_{700} was normalized to zero, the fully oxidized state was normalized to one. Reduced P_{700} was photoxidized by a 200 ms light pulse (6000 µE m^{-2} s^{-1}). After the end of the light pulse, the reduction kinetics of P_{700} were analyzed. As PSI was disconnected from PSII due to detergent treatment, 1 µM PC and 100µM TMPD were added as artificial donor system. Analysis of redox kinetics revealed that the donor side of Δ*psaJ* mutants is highly vulnerable to thylakoid solubilization, because a fraction of slowly reduced P_{700}, which is inaccessible to PC, became apparent after addition of 0.2 % DDM, whereas the PSI donor side function remained unaltered in WT thylakoids.

Figure 5. Unaltered *in vivo* redox kinetics of PC and P_{700} in Δ*psaJ* leaves. PC and P_{700} redox kinetics were measured in intact WT and Δ*psaJ* leaves (leaves number four from the top). The reduced states of PC and P_{700} were normalized to zero, the fully oxidized states of both components were normalized to one. The "high-potential chain" comprising cyt-f, PC and P_{700} was fully oxidized by a strong light-pulse (200 ms duration, 6000 µE m^{-2} s^{-1} intensity), and the PSII side of the electron transport chain was concomitantly reduced. (A) Reduction kinetics. At time point 0, the saturating light pulse was switched off, and dark reduction of PC and P_{700} by electrons from the PQ pool was traced. PC and P_{700} reduction kinetics of WT and Δ*psaJ* plants are about identical, with average P_{700} reduction halftimes of 3.5 ms. PC reduction was slower, as expected due to its lower redox potential relative to P_{700}. P_{700} signals of WT are given as filled circles, and PC signals are given as filled boxes. Δ*psaJ* signals are presented as open circles (P_{700}) and open boxes (PC), respectively. (B) To analyze the interaction of PC and P_{700} quantitatively, the normalized PC (Y-axis) and P_{700} (X-axis) reduction kinetics were

plotted against each other, and the apparent redox equilibration constants were calculated. For both WT and Δ*psaJ*, identical k_{app} values in the range of 7.5 were obtained.

Figure 6. PSI excitation in the *psaJ* knockout mutant is less efficient in low light. (A) The steady state redox state of the PQ pool was analyzed at light intensities between 0 and 700 µE m^{-2} s^{-1}. At low light intensities, PQ is considerably more reduced in the Δ*psaJ* mutant (PsaJ) than in the WT (WT), despite identical maximum capacities of linear electron flux. The more reduced redox state of the PQ pool under light-limited conditions indicates a lower rate of PQ oxidation (that is, PSI excitation and photochemistry), than reduction (i.e., PSII excitation and photochemistry). (B) Phenotype of the Δ*psaJ* mutant under low light conditions. To confirm the reduced efficiency of photosynthesis in the mutants under light-limited conditions, WT and mutant plants were grown at 20 µE m^{-2} s^{-1}. When grown under these low light conditions for two weeks, the mutants (right plant) show retarded growth and reduced chl. content per leaf area compared to the WT control (left plant).

Figure 7. Immunoblot analysis of marker proteins for the antenna system. The first four lanes of each blot show undiluted WT thylakoids from leaves number 4, and dilutions to 50%, 20% and 10% of the undiluted WT sample, to determine the response range of the antibody. The next four lanes display WT thylakoids isolated from leaves four (lane 5), six (lane 6), nine (lane 7) and eleven (lane 8). Lanes 9 to 12 show thylakoids isolated from the corresponding mutant leaves. Whereas no significant differences between WT and Δ*psaJ* mutant were obtained for Lhcb proteins and the majority of Lhca proteins, the accumulation of Lhca3 was clearly reduced in the mutants.

Figure 8. Altered PSI chl.-a fluorescence emission signals of Δ*psaJ* mutants at 77 K. Chl.-a fluorescence of isolated thylakoids equivalent to 10 µg chl. ml^{-1} was excited at 430 nm. Fluorescence emission of PSII at 686 nm wavelength was normalized to one. WT thylakoids (WT) show a typical 77 K chl.-a fluorescence emission spectrum, with a PSI emission maximum at 733 nm wavelength. In the Δ*psaJ* mutant (PsaJ), the overall fluorescence emission of the PSI antenna system was reduced, in agreement with reduced PSI and Lhca3 contents. Also, the maximum was blue-shifted from 733 nm to 728 nm, indicating an altered functional PSI antenna organization.

Figure 1:

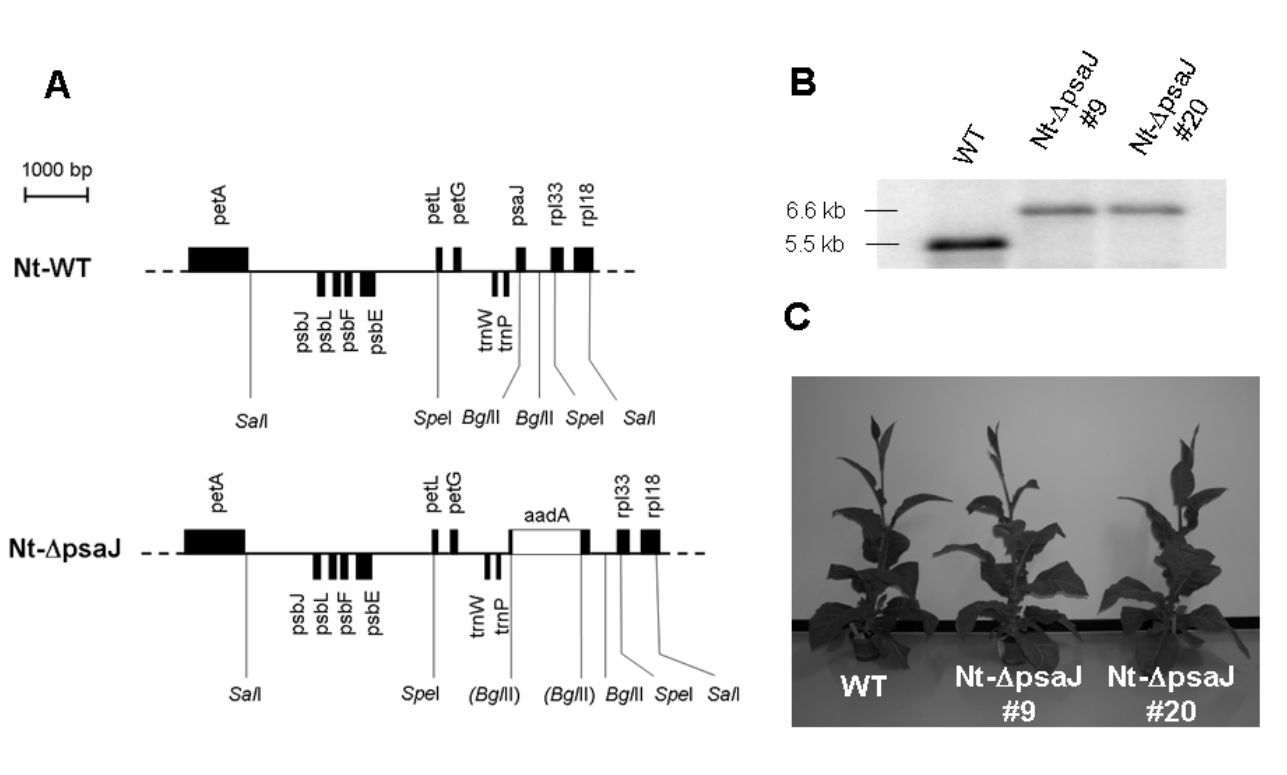

Figure 2:

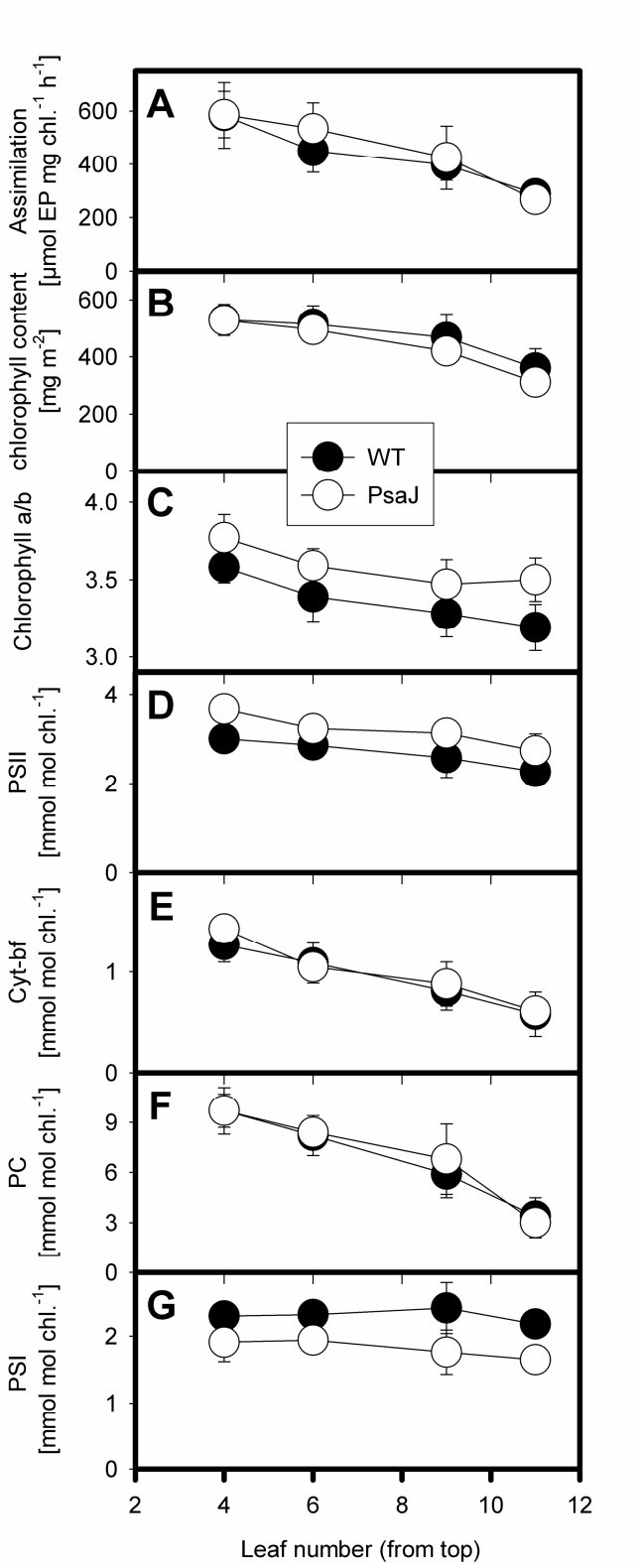

Figure 3:

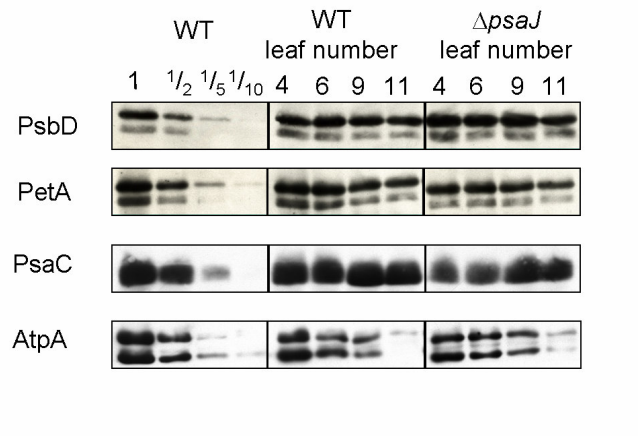

Figure 4:

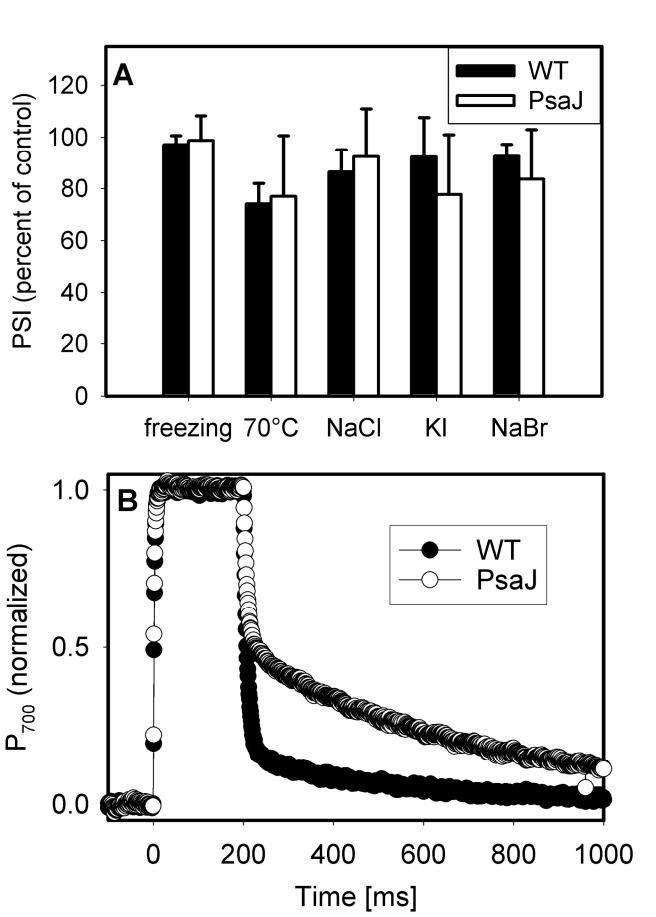

Figure 5:

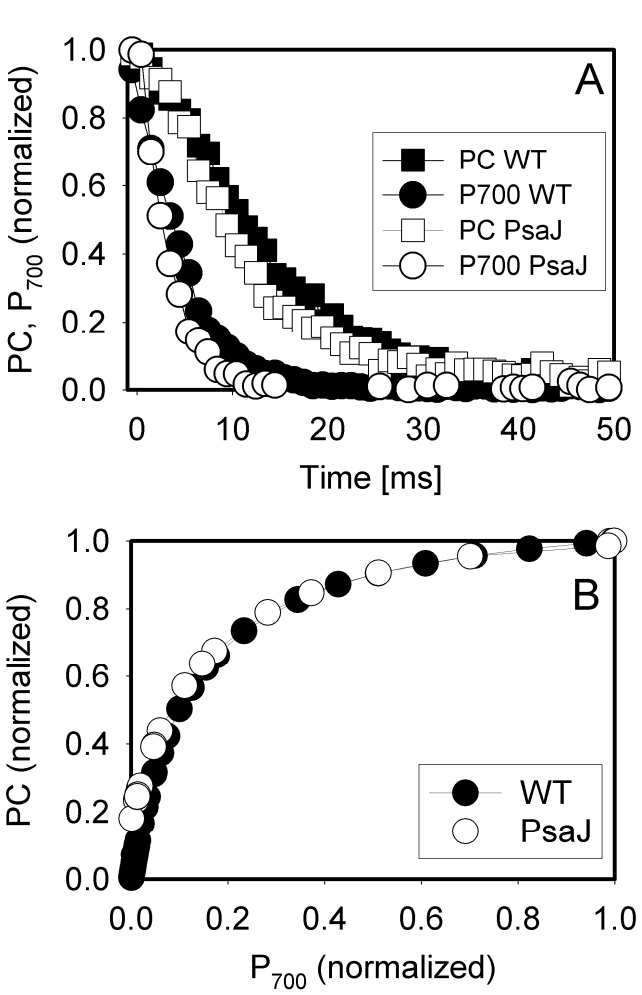

Figure 6:

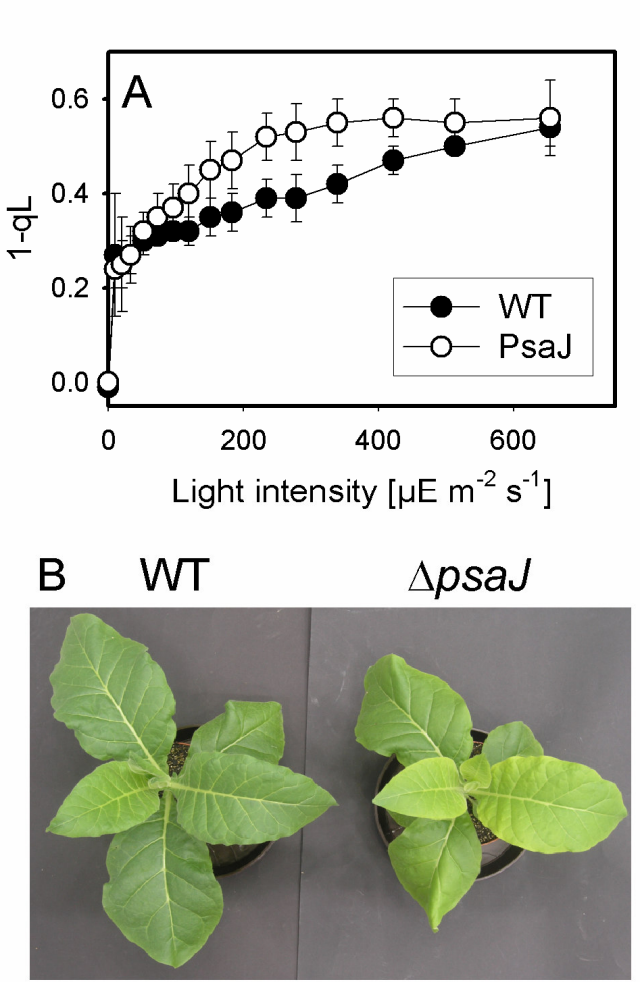

Figure 7:

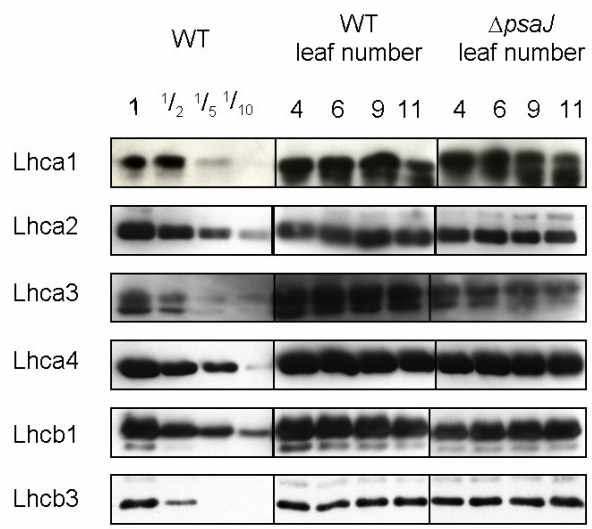

Figure 8: